https://doi.org/10.5194/acp-2019-573
Preprint. Discussion started: 19 July 2019

Atmospheric Chemistry and Physics Discussions

Comparison of IAGOS in-situ water vapour measurements and ECMWF ERA-Interim Reanalysis data

Philipp Reutter[1], Patrick Neis[1,2,*], Susanne Rohs[2], and Bastien Sauvage[3]

[1]Institute for Atmospheric Physics, Johannes Gutenberg University Mainz, Mainz, Germany
[2]Institute of Energy and Climate Research Troposphere (IEK-8), Forschungszentrum Jülich, Jülich, Germany
[3]Laboratoire d'Aerologie, Paul Sabatier University Toulouse, Toulouse, France
[*]now at: CGI Deutschland

Correspondence: Philipp Reutter (preutter@uni-mainz.de)

Abstract. Cirrus clouds and their potential formation regions, so-called ice-supersaturated regions (ISSRs) occur frequently in the tropopause region. It is assumed that ISSRs and cirrus clouds can change the tropopause structure by diabatic processes, driven by latent heating due to phase transition and interaction with radiation. For many research questions a three-dimensional picture including a sufficient temporal resolution of the water vapour fields in the tropopause region is required. This requirement is fulfilled nowadays by reanalysis products such as the European Centre for Medium-Range Weather Forecasts (ECMWF) ERA-Interim reanalysis. However, for a meaningful investigation of water vapour in the tropopause region a comparison of the reanalysis data with measurement is advisable, since it is difficult to measure water vapour and to assimilate meaningful measurements into reanalysis products. Here, we present an intercomparison of high-resolution in-situ measurements aboard passenger aircraft within the European Research Infrastructure IAGOS (In-service Aircraft for a Global Observing System; http://www.iagos.org) with ERA-Interim. Temperature and humidity data over the North Atlantic from 2000 to 2010 are compared relative to the dynamical tropopause. The comparison of the temperature shows a good agreement between measurement and ERA-Interim. While ERA-Interim also shows the main features of the water vapour measurements of IAGOS, the variability of the data is clearly smaller in the reanalysis data set. The combination of temperature and water vapour leads to the relative humidity with respect to ice ($\mathrm{RH_i}$). Here ERA-Interim deviates from the measurements concerning values of larger than $\mathrm{RH_i} = 100\,\%$, both in number and strength of supersaturation. The comparison of ISSR pathlengths shows distinct differences, which can be traced back to the spatial resolution of both data sets. IAGOS shows significantly more smaller ISSRs compared to ERA-Interim. A good agreement begins only at pathlengths in the order of the ERA-Interim spatial resolution and larger.

1 Introduction

Water vapour is the most important greenhouse gas in the atmosphere and therefore plays a major role in the Earth's radiative balance (Myhre et al., 2013). Especially in condensed form water is also of large significance for the planetary radiation. Clouds can reflect incoming solar radiation, while absorbing and reemitting longwave radiation from the earth. Particularly the effect of cirrus clouds are still challenging. Whether a cirrus clouds has a net warming or cooling effect on the Earth's atmosphere

https://doi.org/10.5194/acp-2019-573
Preprint. Discussion started: 19 July 2019

Atmospheric Chemistry and Physics Discussions

depends strongly on altitude, available humidity and microphyiscal properties like number, size and type of ice nuclei (IN). Even the same exact cirrus cloud can change the sign of its net forcing depending on the time of day (Joos et al., 2014).

The control parameter for cold cloud formation in the upper troposphere is relative humidity with respect to ice, which reaches supersaturation by exceeding the temperature dependent water-holding capacity of the air mass (Gierens and Spichtinger, 2000; Spichtinger et al., 2003).

$$\mathrm{RH_i} = 100 \cdot \frac{p_\mathrm{v}}{p_\mathrm{si}(T)} \tag{1}$$

where p_v is the present water vapour partial pressure and p_si the water vapour saturation pressure over ice water at temperature T, respectively. The amount of ice supersaturation needed to form ice crystals depends strongly on the nucleation mechanism. Homogeneous nucleation of solution droplets requires supersaturations with respect to ice of at least $45\,\%$ (Koop et al., 2000), whereas heterogeneous freezing occurs at much lower supersaturations (DeMott et al., 2003; Mohler et al., 2006).

Ice supersaturation, first hypothesized by Alfred Wegener in 1911, is commonly found in the upper troposphere (Gierens et al., 1999; Spichtinger and Leschner, 2016; Gettelman et al., 2006).

Therefore, the so-called ice supersaturated regions (ISSR) constitute an important formation region for in-situ cirrus clouds (Krämer et al., 2016). While ISSRs alone do only have a minor effect on the local radiative budget (Fusina et al., 2007), the transformation from an ISSR to a region with cirrus clouds has a significant effect.

Although ISSRs and cirrus clouds are mostly found in the upper troposphere, they also occur above the tropopause and have an effect on the lower stratosphere (LS). Since the region of the upper troposphere and lower stratosphere, the so-called UTLS region, is characterized by the coldest and driest air (Dessler and Sherwood, 2009; Held and Soden, 2000) the outgoing long-wave radiation is most sensitive to absolute changes in the UTLS water vapour (Riese et al., 2012).

Besides the major role in the planetary radiation balance, water vapour distributions in the upper troposphere and lower stratosphere influences the UTLS chemistry. For example, stratospheric water vapour is partly a product of photochemical methane oxidation and will increase with anthropogenically increasing tropospheric methane concentrations (Rohs et al., 2006). This increase of water vapour could lead to a more frequent formation of polar stratospheric clouds causing more ozone destruction in the stratosphere (Solomon et al., 2010). The chemical impact of tropospheric water vapour is, for example, the reaction with photolyzed ozone to the hyydroxyl radical OH which further reacts with hundreds of gases and also leads to the rapid formation of acids that are deposit in precipitation (Thompson, 1992).

Another important aspect of water vapour distribution in the atmosphere is its feedback on atmospheric motions and stability. Water vapour is transported quickly through the atmosphere and redistributes energy by phase changes. For example, the condensation of water vapour close to the tropopause in potentially unstable layers can trigger the so-called shallow cirrus convection by latent heat release (Spichtinger, 2014). This alters the temperature and stability close to the tropopause with further implications on the exchange of air masses between troposphere and stratosphere.

Hence, a thorough description of processes related to the water vapour distribution are of crucial importance. However, measurements of water vapour at the tropopause level are not trivial. Beside radiosonde data the most important in-situ data set is provided by in-service passenger airplanes. Since 1994, commercial passenger aircrafts are measuring water vapour

https://doi.org/10.5194/acp-2019-573
Preprint. Discussion started: 19 July 2019

Atmospheric Chemistry and Physics Discussions

in the UTLS within the framework IAGOS (In-service Aircraft for a Global Oberserving System, (Petzold et al., 2015)) and its predecessors MOZAIC (Measurement of Ozone and Water Vapour on Airbus in-service Aircraft, (Marenco et al., 1998)) and CARIBIC (Civil Aircraft for the Regular Investigation of the Atmosphere Based on an Instrument Container, (Brenninkmeijer et al., 2007)). These regular measurements on a global scale are unique in their quantity, continuity and quality of measurements. Using five years of the continuous measurements over the North Atlantic, Gierens et al. (1999) described the humidity distribution in this region. These results were then used to improve the cloud scheme in the European Centre for Medium-Range Weather Forecast (ECMWF) Integrated Forecast Model (IFS) including the parameterization of superaturation with respect to ice in the cloud-free part of the grid box (Tompkins et al., 2007)

Meanwhile, the IAGOS data set now spans about 20 years and also allows trend analysis, for example with regard to the temperature. Here, a difference between in-situ and modelled data arise. While IAGOS exhibits a neutral temperature trend in the LS, the reanalysis data ERA-Interim of the ECMWF shows a temperature trend of $+0.56\,\mathrm{K\,decade^{-1}}$ (Berkes et al., 2017). This underlines the importance of a thorough comparison between measurements and modelled data. To investigate the mutual influence of water vapour in the UTLS region in the future, properties regarding the water vapour such like relative humidity with respect to ice, fraction of ice supersaturated regions or pathlengths of ISSRs are compared between IAGOS measurements and ERA-Interim output. A companion study by Neis et al (in preparation) will focus on the physical interpretation of the water vapour distribution in the UTLS region. The aim of this work is to asses the quality of the desription of water vapour in the UTLS region in the ERA-Interim data set.

Therefore, the data sets ranging from 2000 to 2010 are compared. Sect. 2 describes the data sets and the methodology. In Sect. 3 the comparison of IAGOS and ERA-Interim is presented in different ways. The conclusion can be found in Sect. 4.

2 Data and methodology

The evaluation of the reanalysis data is based on in-situ measurements. Both data sets are presented in the following.

2.1 IAGOS

The European Research Infrastructure 'In-service Aircraft for a Global Observing System' (IAGOS, Petzold et al. (2015)) provides long-term in-situ measurements in the UTLS region. The IAGOS-CORE component, successor of the MOZAIC part, comprises the implementation and operation of autonomous instruments installed on long-range aircraft of internationally operating airlines for continous, global-scale and daily measurements of reactive gases and long-lived greenhous gases (e.g. CO, $\mathrm{CO_2}$, $\mathrm{CH_4}$ and water vapour), important chemically active trace gases (e.g. $\mathrm{O_3}$), as well as aerosol, dust and cloud particles (Bundke et al., 2015; Filges et al., 2015).

Especially in the UTLS region these measurements are very valuable as most flight tracks are situated in heights between 9 to $13\,\mathrm{km}$, depending on the actual weather conditions, seasons and geographic region.

Starting from August 1994 more than 60000 flights (May 2019) have been performed, including data from the IAGOS predecessor MOZAIC (August 1994 to December 2014) and data from the IAGOS project starting in July 2011 until present.

https://doi.org/10.5194/acp-2019-573
Preprint. Discussion started: 19 July 2019

Atmospheric Chemistry and Physics Discussions

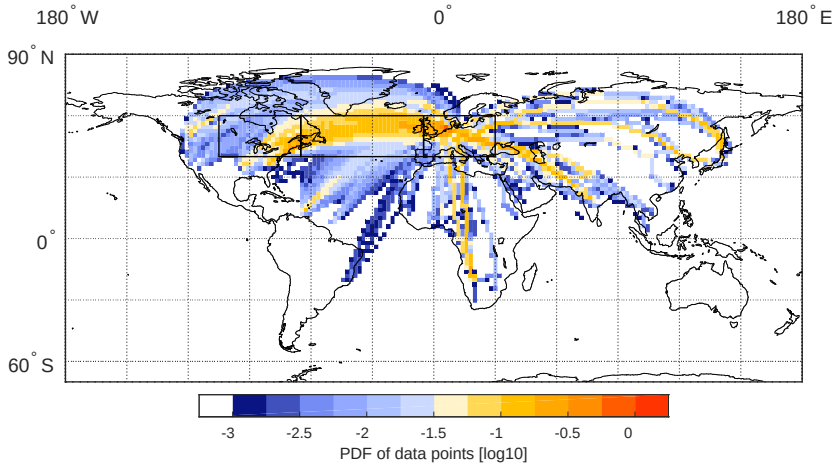

Figure 1. Geographic distribution of IAGOS observations shown as probability distribution function of data points in values of the decadal logarithm of % of data. The best coverage occurs over the North Atlantic flight corridor.

From Figure 1 it is obvious that the global data distribution is not uniform in every region. The subset covering the North Atlantic flight corridor shows the highest coverage of flights. Therefore, in our study we focus on this region (40N-60N, 5-65W). For the evaluation of the reanalysis data we use the geographic position of the airplane (lat/lon), the time, data quality flags, ambient pressure and temperature (Berkes et al., 2017), relative humidity and water vapour volume mixing ratio. In this study we use the data collected during January 2000 to December 2010. For further information regarding the IAGOS project the reader is referred to the project's website www.iagos.org and the references therein.

2.2 ERA-Interim

For this study the ERA-Interim reanalysis data set from the European Centre of Medium-Range Weather Forecasts (ECMWF) is used (Dee et al., 2011). The spectral resolution of the underlying IFS model from 2006 is T255, which calculates to a horizontal resolution of about $80\,\mathrm{km}$. The vertical dimension is separated into 60 levels reaching from the surface up to a pressure level of $0.1\,\mathrm{hPa}$.

For the comparison with the IAGOS measurements the 6-hourly ERA-Interim data were previously converted on a $1°$ horizontally grid and interpolated on pressure levels (Kunz et al., 2014). Then, the fields of temperature, pressure and specific humidity are projected on the aircraft's flight path by linear spatial and temporal interpolation. Finally, the data is available with a $4\,\mathrm{s}$ resolution along the flight track (Berkes et al., 2017).

The relative humidity with respect to ice was calculated using the approximation by Murphy and Koop (2005). As mentioned already in the introduction, the ERA-Interim data set was obtained by using the IFS model including the so-called Tompkins scheme (Tompkins et al., 2007), which allows for the supersaturation with respect to ice in cloud-free regions. However, inside

https://doi.org/10.5194/acp-2019-573
Preprint. Discussion started: 19 July 2019

Atmospheric Chemistry and Physics Discussions

Region	Shortname	$p_{\mathrm{ap}} - p_{\mathrm{tph}}$ [hPa]
Lowermost stratosphere	LS3	-90
	LS2	-60
	LS 1	-30
Tropopause layer	TL	0
Uppermost troposphere	UT1	+30
	UT2	+60
	UT3	+90

Table 1. The data set is distributed into three main layers: the upper troposphere, tropopause layer, and lowermost stratosphere. The outer layers are additionally subdivided into three sublayers. The distribution criterion is the pressure difference between aircraft pressure p_{ac} and the tropopause pressure p_{tph} with the range of $\pm 15\mathrm{hPa}$.

of cirrus clouds an occurring supersaturation is adjusted down to $100\,\%$. In the following we use ERA to label the ERA-Interim data.

2.3 Methodology

Aircraft based measurements of atmospheric state variables and chemical composition usually refer to the aircraft flight altitude or pressure level, respectively. In the present work the humidity data will be separated relative to the tropopause height in order to study the humidity in the tropopause region. We use the dynamical tropopause, which is defined by a sharp gradient in the potential vorticity (PV). The here used value to define the tropopause is PV = 2 PVU (1 PVU $= 10^6\,\mathrm{K\,m^2\,kg^{-1}\,s^{-1}}$, standard potential vorticity unit) (Holton, 2005). A former study (Neis, 2017) showed that the choice of the tropopause definition can have an important impact on the interpretation of the results. However, in this study we want to compare two data sets. Therefore, the definition of the tropopause plays only a minor role. The vertical data will be distributed into three main layers: upper troposphere (UT), tropopause layer (TP), and lower stratosphere (LS) in accordance to Thouret et al. (2006). Furthermore, UT and LS are each separated into three subclasses. The width of the sublayers consider the average difference between ozone and thermal tropopause of $780\,\mathrm{m}$ ($30\,\mathrm{hPa}$ at this altitude) (Bethan et al., 1996). The resulting seven $30\,\mathrm{hPa}$ thick bins separate the aircraft pressure relative to the tropopause pressure and are summarized in Table 1.

Before the distribution of the data several filters are applied. First, the measured data must lie within the geographic region from $40\,^\circ$ to $60\,^\circ$ North and $-65\,^\circ$ to $5\,^\circ$ East. All data must be collected in a height above $350\,\mathrm{hPa}$ and within a temperature range between $233\,\mathrm{K}$ and $200\,\mathrm{K}$ corresponding to the threshold of homogeneous freezing (Heymsfield and Sabin, 1989) and calibration limit of the humidity sensor (Neis, 2017), respectively. Additionally, the relative humidity with respect to liquid water must be below $100\,\%$ and several measurement quality flags must be fulfilled. The above mentioned criteria are applied to both data sets and is the starting point of the comparison.

https://doi.org/10.5194/acp-2019-573
Preprint. Discussion started: 19 July 2019

Atmospheric Chemistry and Physics Discussions

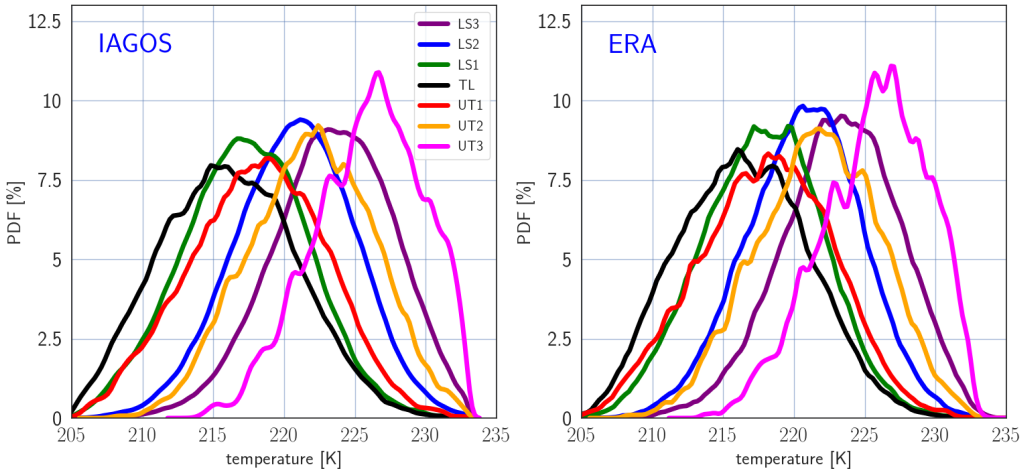

Figure 2. Vertical distribution of temperature [K] for (left) IAGOS and (right) ERA from the year 2000 to 2010. The different heights levels are color coded.

Layer	Median temperature [K]		Mean temperature [K]		Standard deviation [K]	
	IAGOS	ERA	IAGOS	ERA	IAGOS	ERA
LS3	223.5	223.4	223.4	223.3	4.2	4.1
LS2	220.8	220.8	220.7	220.7	4.3	4.0
LS1	217.3	217.9	217.3	217.8	4.4	4.2
TL	216.0	216.4	216.1	216.5	4.7	4.5
UT1	218.3	218.1	218.1	218.0	4.8	4.7
UT2	222.0	221.8	221.9	221.7	4.4	4.3
UT3	226.2	226.0	225.9	225.7	3.8	3.7

Table 2. Median, mean and standard deviation of temperature [K] for IAGOS and ERA data. The comparison shows a very good agreement.

3 Results

The aim of this study is to compare and quantify the difference of relative humidity with respect to ice (RH_i) between the in-situ measurements provided by IAGOS and the reanalysis data of ERA-Interim.

3.1 Temperature

https://doi.org/10.5194/acp-2019-573
Preprint. Discussion started: 19 July 2019

Atmospheric Chemistry and Physics Discussions

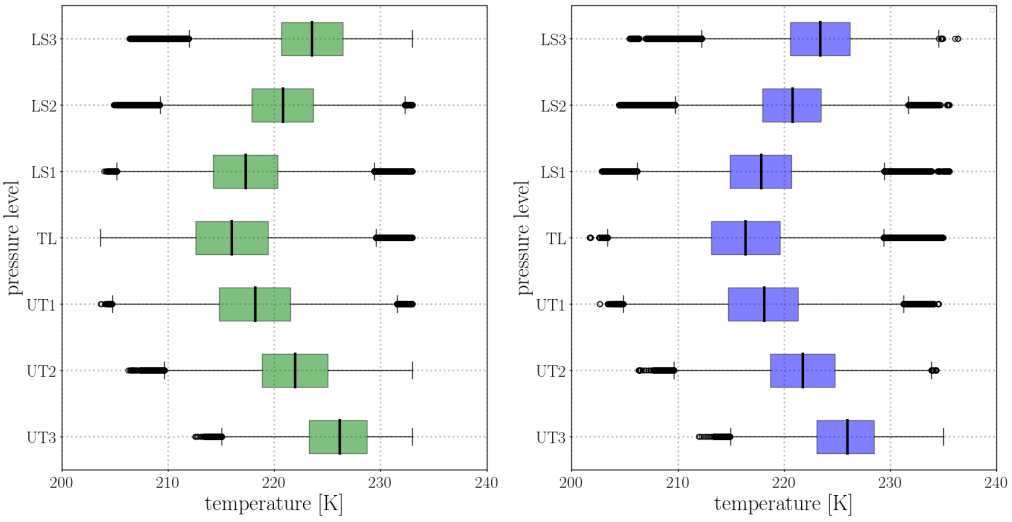

Figure 3. Vertical profile of temperature [K] for IAGOS (left) and ERA (right).

According to Equation 1 the relative humidity depends on temperature and available water vapour. Figure 2 shows the temperature probability density function (PDF) in the seven vertical layers for IAGOS and ERA. With exception of layer UT3, the distributions show a quasi-Gaussian behaviour. As expected by definition, the tropopause layer shows the coldest mean temperatures with 216.1 K and 216.5 K for IAGOS and ERA, respectively. The warmest mean temperatures are visible for the lowest layer UT3 with about 225 K in both cases. The origin of the "wave-like" structure of the distribution at the UT3 layer is not clear. One reason might be that in this layer, well inside the troposphere, a variety of dynamic and diabatic processes occur. Overall, the comparison between IAGOS and ERA shows a good agreement as far as the statistical values are concerned (see Table 2).

Figure 3 shows the vertical profile of the temperature for IAGOS and ERA in the form of a Box-and-Whisker plot. The boxes are bounded by the 25 % and 75 % percentile, while the median is marked with a black vertical line. The whiskers are defined as $1.5 \cdot$ IQ with IQ the interquartile range, being equal the distance between the 25 % and 75 %. Outliers, values exceeding the whiskers, are marked as black circles. A very good agreement between the temperature in IAGOS and ERA-Interim is seen, highlighted by the symmetry of both profiles. Additionally, the boxes of the box-and-whisker plots are equal in size, pointing to a similar statistics of the data set. As expected, for both data sets the minimal temperature is found in the tropopause layer.

3.2 Water vapour

https://doi.org/10.5194/acp-2019-573
Preprint. Discussion started: 19 July 2019

Atmospheric Chemistry and Physics Discussions

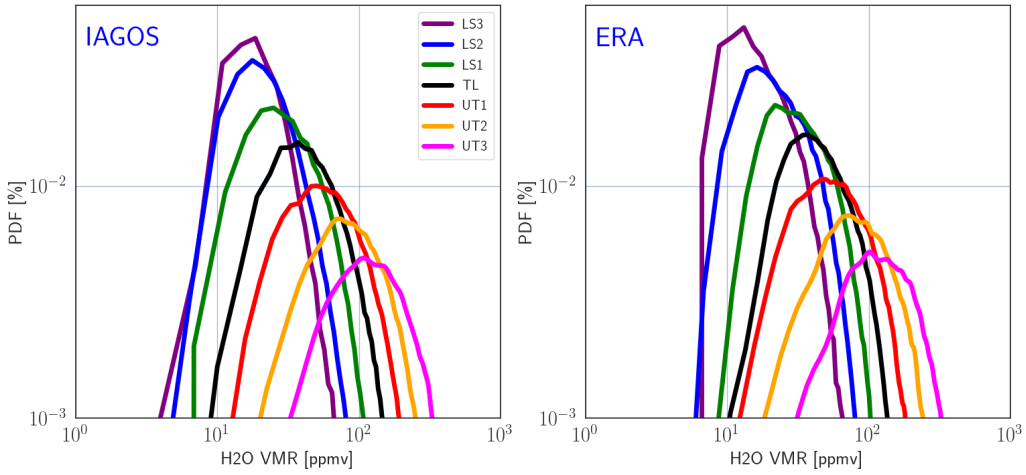

Figure 4. Vertical distribution of water vapour volume mixing ratio [ppmv] for (left) IAGOS and (right) ERA.

Layer	Median VMR [ppmv]		Mean VMR [ppmv]		Standard deviation [ppmv]	
	IAGOS	ERA	IAGOS	ERA	IAGOS	ERA
LS3	20	19	24	22	16.8	14.7
LS2	25	27	29	31	19.6	17.9
LS1	36	38	42	43	26.6	23.2
TL	52	52	61	31	37.5	31.1
UT1	75	71	87	81	51.8	44.5
UT2	110	106	125	118	70.2	62.8
UT3	158	154	176	167	95.4	83.6

Table 3. Median, mean and standard deviation of water vapour volume mixing ratio [ppmv] for IAGOS and ERA data. The comparsion shows a very good agreement.

https://doi.org/10.5194/acp-2019-573
Preprint. Discussion started: 19 July 2019

Atmospheric Chemistry and Physics Discussions

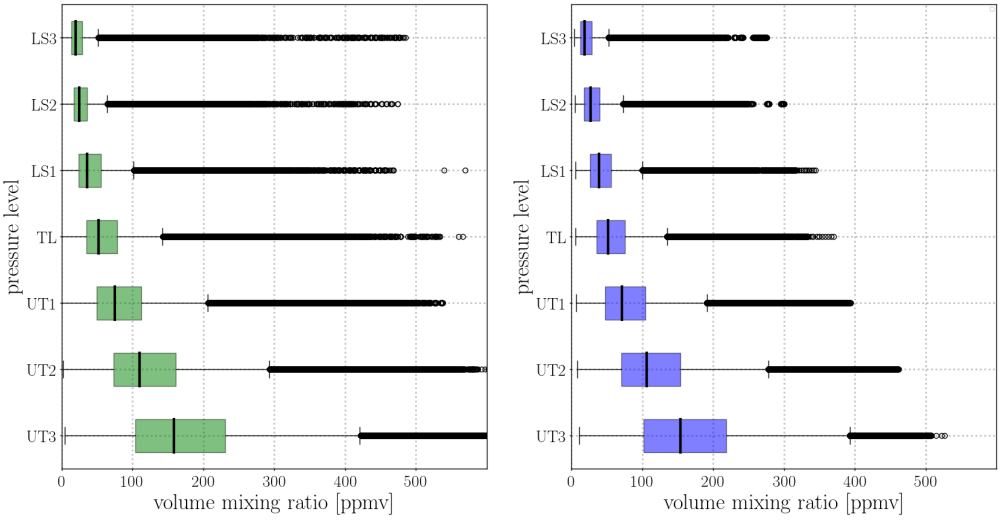

Figure 5. Vertical profile of H_2O volume mixing ratio [ppmv] for IAGOS (left) and ERA (right).

The probability densitiy function of the water vapour volume mixing ratio is presented in Fig. 4. Here, a clear dependence of the distribution with height is visible. Note, due to the broadening of the distribution with decreasing height, the absolute probabilities are decreasing in this log-log illustration. The lowest mean and median values of the water vapour volume mixing ratio are observed, as expected, in the uppermost layer LS3. In contrast, the lowermost level UT3 shows the largest mean values of the water vapour mixing ratio. The comparison between IAGOS and ERA shows a good overall agreement (see Table 3). However, very low volume mixing ratios seem to be hard to achieve for the ERA model, which is visible for the two uppermost levels LS2 and LS3. It is also noteworthy that for the upper layers, beginning from the tropopause layer up to LS3, the left part of the distributions show always a much steeper behaviour in the ERA data set compared to IAGOS. Hence, ERA shows less variability of water vapour in the tropopause region and above.

Figure 5 shows the vertical structure of the water vapour mixing ratio. For the upper layers in both data sets starting from the tropopause level (TL) up to LS3 the variability, i.e. the size of the boxes, is significantly lower compared to the tropospheric layers (UT1 to UT3). Overall it can be stated that the variability is increasing with decreasing height. As mentioned before, the variability of the reanalysis data set is also smaller for the upper layers compared to the in-situ data. When focussing on absolute numbers it is also visible that IAGOS data set shows higher maximum values in the stratosphere compared to ERA. In summary, the reanalysis data is in good agreement with the vertical distribution and the seasonal cycle of the IAGOS data beside the smaller variability and extreme values of the in-situ data.

https://doi.org/10.5194/acp-2019-573
Preprint. Discussion started: 19 July 2019

Atmospheric Chemistry and Physics Discussions

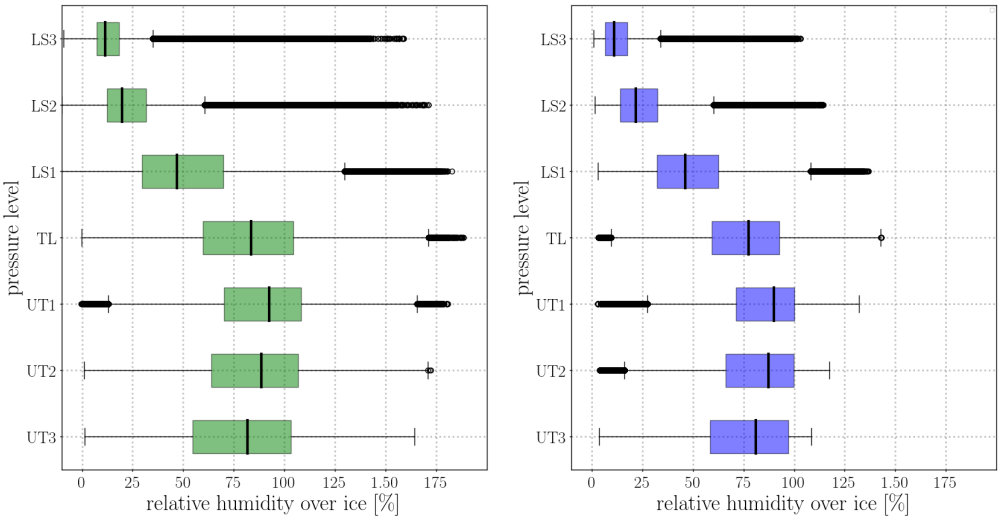

Figure 6. Vertical profile of relative humidity with respect to ice (RHi) [%] for IAGOS (left) and ERA (right).

Layer	Median RHi [%]		Mean RHi [%]		Standard deviation RHi [%]	
	IAGOS	ERA	IAGOS	ERA	IAGOS	ERA
LS3	12	11	15	14	12	10
LS2	20	22	24	25	17	15
LS1	47	46	52	48	29	22
TL	84	77	82	75	29	22
UT1	93	90	86	84	27	20
UT2	89	87	85	81	28	22
UT3	82	81	79	76	30	23

Table 4. Median, mean and standard deviation of RHi [%] for IAGOS and ERA. The comparison shows a good agreement.

3.3 Relative humidity with respect to ice

Since cloud formation is governed by the relative humidity rather than the water vapour mixing ratio the relative humidity w.r.t. ice RH_i is now investigated. As mentioned in the introduction, RH_i depends on both temperature and available water vapour. Hence, relative humidity is a convolution of both variables. In Fig. 6 the vertical structure of RH_i is depicted. The overall results show two different regimes. In the troposphere up to the tropopause layer the statistics cover the whole range of possible saturation values. $50\,\%$ of the data, indicated by the boxes, of each layer from UT3 to TL are situated between

https://doi.org/10.5194/acp-2019-573
Preprint. Discussion started: 19 July 2019

Atmospheric Chemistry and Physics Discussions

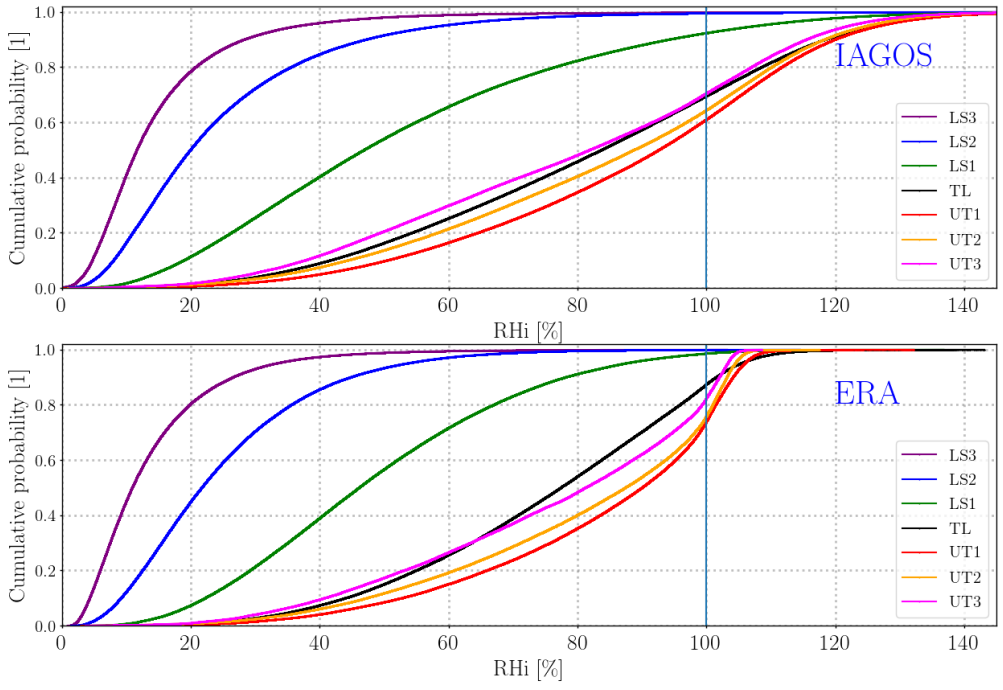

Figure 7. Cumulative distribution of $\mathrm{RH_i}$ for every height level in the IAGOS (top) and ERA (bottom) data set. The vertical blue line denotes saturation w.r.t. ice.

$50\,\%$ and $100\,\%$ $\mathrm{RH_i}$. The highest median values are found in the layer UT1 for both data sets. In the tropopause layer still a significant amount of the data are exceeding values of $\mathrm{RH}_i > 100\,\%$, both in the in-situ data as well as in the ERA data set. However, the whisker in Fig. 6 indicate that ERA has less data points with a higher supersaturation compared to IAGOS. In the stratospheric layers the median of the RH_i values is decreasing strongly. However, ice supersaturation is still possible, especially in the lowest stratospheric layer LS1 (Müller et al., 2015). The statistics of ISSRs in higher levels provided by the ERA data set shows clearly less occurrence of this feature. This has important implications on the radiative impact of these layers on the Earth's radiative budget, if climate models underestimate the abundance of ISSRs.

It is obvious that ERA and IAGOS show a good agreement for situations below ice supersaturation. However, in this study we focus on the situation where ice supersaturation exists. For a more distinct look on the occurrence of ISSR we illustrate the statistic evaluation with cumulative probability distributions. Figure 7 shows the cumulative distributions for IAGOS and ERA. Each layer is depicted with its own color. It is clearly visible that ERA and IAGOS behave differently for $\mathrm{RH}_i > 1$, especially for the tropospheric layers. The ERA distributions of the latter layers snap off as soon as they reach ice supersaturation. As mentioned before, the IFS-model allows the existence of ice supersaturation, but only in cloud free conditions. As soon as ice

https://doi.org/10.5194/acp-2019-573
Preprint. Discussion started: 19 July 2019

Atmospheric Chemistry and Physics Discussions

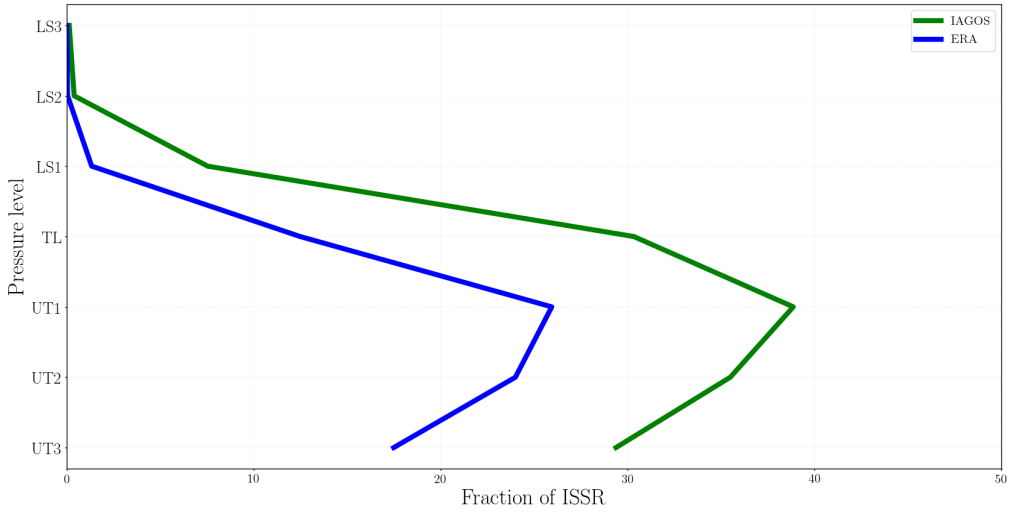

Figure 8. Vertical profile of the fraction of ice supersaturated regions for IAGOS (green) and ERA (blue)

clouds are present in the models grid cell the supersaturation is adjusted to $\mathrm{RH}_i = 100\%$. Unfortunately, the IAGOS data set of the investigated time frame cannot distinguish between cloudy and non-cloudy areas. [1] Nevertheless, also in ice clouds ice supersaturation is present (Krämer et al., 2016). Therefore, the behaviour of the cumulative distributions for ERA, especially in the layers from UT3 to TL, points to a missing process in the representation of ice supersaturation in the underlying IFS model.

Another way to compare the representation of the water vapour is the fraction of ISSRs. Figure 8 presents the vertical profil of the ISSR fraction. It is clearly visible that the measurements by IAGOS show a higher fraction of ISSR. Only for the two uppermost layers the fraction of both data sets are of comparable magnitude. Here, the very dry conditions produce only in very few cases supersaturation. The largest difference between measurement and reanalysis data occur in the the tropopause layer and the flanking UT1 layer, where a high percentage of ice clouds can be expected. IAGOS shows in the latter layer an ISSR fraction of up to 40%. Since ISSR are a prerequisite for the formation of in-situ cirrus clouds, a misrepresentation of the feature can lead to great deviations in the local radiative budget and can build up to large errors in the local dynamics.

3.4 Horizontal scales of ice supersaturated regions

The horizontal scale of ISSRs offers another possibility to compare the measurements of the IAGOS project with the reanaylsis data from ERA. Former studies (Diao et al., 2014; Spichtinger and Leschner, 2016) showed that the horizontal pathlengths can reach from the very small scale in the order of hundred meters to up to $1000\,\mathrm{km}$. Here, small scale variability will lead to very

[1] Nowadays, the IAGOS setup includes an optical sensor for registration of clouds on the flight path.

https://doi.org/10.5194/acp-2019-573
Preprint. Discussion started: 19 July 2019

Atmospheric Chemistry and Physics Discussions

short ISSRs, while large scale features will produce large ISSR pathlenghts. It is obvious that the smallest possible pathlength of the ERA data set is limited by the models spatial resolution. However, by calculating a moving average of the data close to the ERA resolution a comparison is possible. Additionally, we want to answer the question, which resolution is necessary in order to receive a helpful representation of the horizontal scales of ISSRs. A comprehensive representation of ISSRs in atmospheric models enables further investigations on the linkage between small-scale variability and large-scale features.

3.4.1 Examples of ISSR representations during two different flights

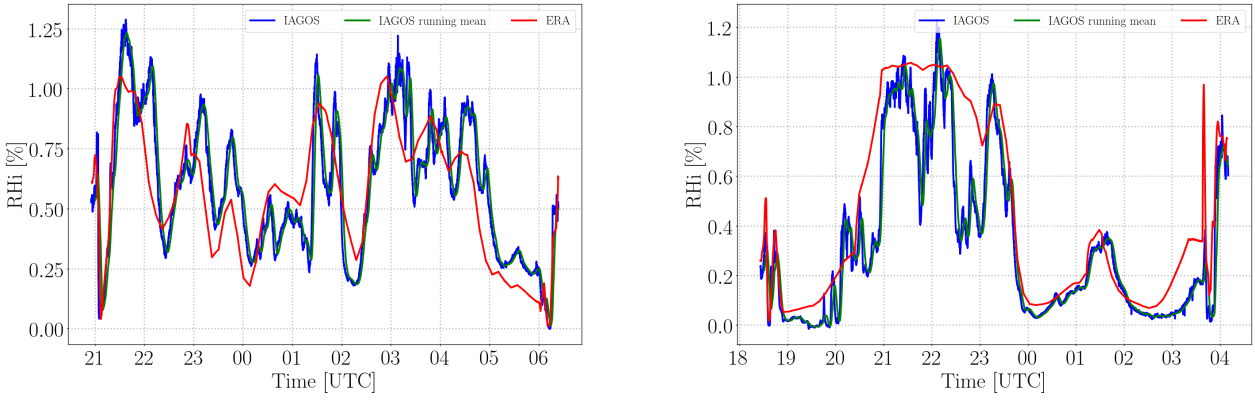

Figure 9. Two flight paths showing RH_i for (blue) IAGOS, (red) ERA and (green) coarse IAGOS data (100 km). Left flight shows a good agreement between small and large scale features. Right flight shows a good representation of larger scales but without small scale features.

Figure 9 presents two flights of the IAGOS data set. Blue shows the high resolution data available from the IAGOS data base. Red shows the ERA data obtained from the given flight track and green shows a $100\,\mathrm{km}$ running mean of IAGOS data to mimic a coarse resolution comparable with the ERA spatial resolution. On the left side IAGOS and ERA show a good agreement. While the magnitude of the ice supersaturation cannot be found in ERA, the reanalysis data shows also small scale features of IAGOS. For the other example ERA fails to display the smaller structures within the first half of the flight. However, the large scale feature is described in a useful way by ERA. In both examples the artificially coarse resolution of the IAGOS data set is keeping the small scale information and lacks only the maximum supersaturation.

3.4.2 Histograms of ISSR

Although ISSRs are three-dimensional fields the measurements only provide one-dimensional pathlenghts. For a reasonable comparison between IAGOS and ERA we only evaluate ISSRs on a constant flight level. Figure 10 shows the histograms for the pathlengths of IAGOS, ERA and different running means of the IAGOS data. On the right side, a cumulative distribution is shown. As it is expected from the different underlying resolutions of both data sets, IAGOS shows much more small pathlengths

https://doi.org/10.5194/acp-2019-573
Preprint. Discussion started: 19 July 2019

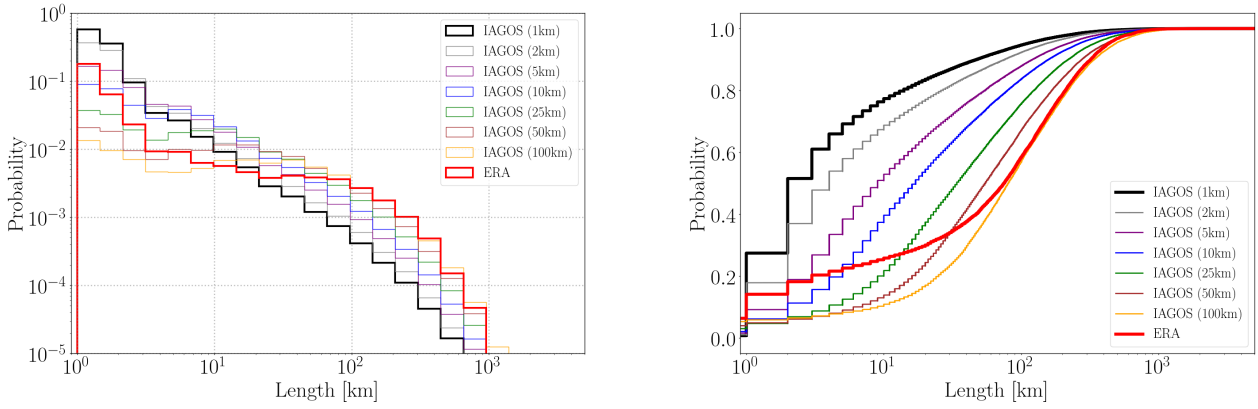

Figure 10. Probability with logarithmic binning (left) and cumulative probability (right)

	IAGOS	ERA-Interim	$IAGOS_{2km}$	$IAGOS_{5km}$	$IAGOS_{10km}$	$IAGOS_{25km}$	$IAGOS_{50km}$	$IAGOS_{100km}$
Median [km]	4	164	7	20	36	74	117	173
Number of ISSRs	107 259	9 751	76 643	49 986	37 811	26 165	19 623	14 732

Table 5. Median values and number of ISSR pathlenghts for IAGOS, ERA-Interim and several running means of the original IAGOS data set.

compared to ERA. On the other side, ERA shows more very large pathlengths larger than 100km. This is especially impressive by looking on the cumulative distribution. Here, the different character of both data sets is most prominent. Comparing the median values given in Table 5 of the original IAGOS data and ERA reveal the big difference. While 50% of the ISSR pathlengths in IAGOS are smaller than 4km, the same threshold for the ERA data set is located at 164km. It has to be noted that due to the lower spatial resolution of the ERA data set only 9751 ISSRs are found compared to 107259 for IAGOS.

The interesting question arises, which theoretical resolution is necessary to describe the ice supersaturation in a sufficient realistic way. Therefore, the IAGOS data is converted not only to a resolution of 100 km but also to further resolutions by using running means of 2, 5, 10, 25 and 50km. Already with a resolution of 1km the cumulative distribution exhibits a different character. Only 35% of the number of ISSR are found compared to the 1km-resolution and the median values increases to 36km. Decreasing the spatial resolution further leads to a decrease in the number of found ISSRs and an increase of the median ISSR pathlength. When reaching a running mean of 100km, which is around the spatial resolution of the ERA data set, the number of found ISSRs and median pathlength are similiar to the reanalysis data. When comparing the results of the running

https://doi.org/10.5194/acp-2019-573
Preprint. Discussion started: 19 July 2019


Atmospheric Chemistry and Physics Discussions

means with the ERA data set it is also noteworthy that the behaviour of the ERA data set changes for pathlengths of $100\,\mathrm{km}$ and lower. Again, as a reminder, this is the scale of the spatial resolution of ERA.

It is clear that the ISSR with pathlengths smaller than $100\,\mathrm{km}$ are not represented in the ERA model in the same way as the running mean of IAGOS shows it. This discrepancy on the first look may be small. However, as mentioned before, small ISSRs also can have a profound effect as formation region of cirrus clouds. The impact of these smaller ISSRS on the larger scale by changing the dynamics around the tropopause are not clear yet.

4 Conclusions

This study compares the in-situ measurements of temperature and water vapour and subsequent relative humidity with respect to ice in the UTLS region obtained by IAGOS with the reanalysis data set ERA-Interim from the year 2000 to 2010 over the North Atlantic. ISSRs are of special interest in this investigation due to their abundance and importance on the local radiation budget when transformed to a cirrus cloud. Both data sets are separated according to their relative height compared to the dynamical tropopause (2PVU).

The comparison of the temperature shows a good agreement between measurement and reanalysis data. The structure and variability of the vertical temperature distribution is very similar, shown by a very good accordance in median and mean values as well as in the standard deviation.

The water vapour was analyzed using the water vapour mixing ratio. Both data sets show the clear decrease of water vapour with increasing height. In contrast to the measurements ERA shows clearly less variability, indicated by smaller standard deviations in all levels.

The convolution of water vapour and temperature leads to the relative humidity with respect to ice, which governs the cloud formation. Both data sets reproduce two different regimes. In the UT layers including the tropopause layer, the statistics cover the whole range of possible saturation values, where most of the data lie between 50% and $100\%\,\mathrm{RH}_i$. However, ERA deviates from the RH_i measurements concerning values of larger than $\mathrm{RH_i} = 100\,\%$ by showing less data points and weaker supersaturations, impressively depicted by the comparison of cumulative distributions. This is an important finding, because it points to a misrepresentation in ERA of ice supersaturation in the UT and tropopause region, which is the formation region of in-situ cirrus.

Moving up to the stratospheric layers, as expected, the RH_i values are much lower in both data sets. Again, ERA shows less and weaker supersaturations through all levels. Since the LS is very dry, supersaturation occurs rarely and therefore the difference between both data sets is smaller regarding the cumulative distribution. Nevertheless, ERA shows clearly less extreme events.

The strong differences between IAGOS and ERA with respect to ISSRs is also shown by the fraction of ISSR. In the UT and the tropopause region the measurements show a significantly larger fraction of ISSR in the measurements compared to ERA.

The comparison of pathlenghts of ISSRs shows clearly the different resolutions of the two data sets. It is obvious that the high-resolution measurements show more small ISSRs than ERA. Only beginning with pathlenghts in the order of $100\,\mathrm{km}$ the

https://doi.org/10.5194/acp-2019-573
Preprint. Discussion started: 19 July 2019

Atmospheric Chemistry and Physics Discussions

distribution start to have a similar course. This length scale coincides with the horizontal resolution of the underlying ERA model.

Decreasing the resolution of the IAGOS data by running means shows only a good agreement of model and measurement beginning with a running mean of $100\,\mathrm{km}$, which is, as stated, in the order of the model resolution. However, even in the latter case, the structure of the distribution of ISSR smaller than $100\,\mathrm{km}$ is clearly different between IAGOS and ERA. Therefore, a simple increase of the model resolution seems not sufficient. Additionally, the physical processes must be refined carefully for a realistic description of the ice supersaturation in the UTLS region.

Although the new version of reanalysis data from the ECMWF, ERA5, is already available, we conducted this study using ERA-Interim. Many studies in this decade regarding the UTLS region are based on ERA-Interim model output (e.g. Zhan and Wang (2012); Riese et al. (2012); Uma et al. (2014); Madonna et al. (2014); Reutter et al. (2015)). Also, ERA-Interim is still used in many ongoing investigations. Therefore, a comparison between measurements and ERA-Interim is still valuable. Nevertheless, the influence of the spatial resolution on the length and number of ISSRs has been shown in this study impressively. Therefore, the next step is to compare the IAGOS measurements with the higher resolution data of ERA5 ($\Delta x = 31\,\mathrm{km}$. It is likely, that the agreement between measurement and reanalysis data is therefore increased. However, a thorough review is advisable. Subsequently, the new reanalysis data will be used for investigations of physical processes regarding ice supersaturation in the UTLS region.

Author contributions. PR and PN performed the analyses and both wrote the text; PN and SR were in charge of the instrument setup, calibration, and processing of the measurements; BS combined reanalysis data with measurements; BS and SR checked the manuscript.

Competing interests. The authors declare that they have no conflict of interest.

Acknowledgements. Philipp Reutter and Patrick Neis want to thank Peter Spichtinger, Andreas Petzold and Peter Hoor for many helpful discussions.

https://doi.org/10.5194/acp-2019-573
Preprint. Discussion started: 19 July 2019

Atmospheric Chemistry and Physics Discussions

References

Berkes, F., Neis, P., Schultz, M. G., Bundke, U., Rohs, S., Smit, H. G. J., Wahner, A., Konopka, P., Boulanger, D., Nédélec, P., Thouret, V., and Petzold, A.: In situ temperature measurements in the upper troposphere and lowermost stratosphere from 2 decades of IAGOS long-term routine observation, Atmospheric Chemistry and Physics, 17, 12 495–12 508, https://doi.org/10.5194/acp-17-12495-2017, https://www.atmos-chem-phys.net/17/12495/2017/, 2017.

Bethan, S., Vaughan, G., and Reid, S. J.: A comparison of ozone and thermal tropopause heights and the impact of tropopause definition on quantifying the ozone content of the troposphere, Quarterly Journal of the Royal Meteorological Society, 122, 929–944, https://doi.org/10.1002/qj.49712253207, https://rmets.onlinelibrary.wiley.com/doi/abs/10.1002/qj.49712253207, 1996.

Brenninkmeijer, C. A. M., Crutzen, P., Boumard, F., Dauer, T., Dix, B., Ebinghaus, R., Filippi, D., Fischer, H., Franke, H., Frieß, U., Heintzenberg, J., Helleis, F., Hermann, M., Kock, H. H., Koeppel, C., Lelieveld, J., Leuenberger, M., Martinsson, B. G., Miemczyk, S., Moret, H. P., Nguyen, H. N., Nyfeler, P., Oram, D., O'Sullivan, D., Penkett, S., Platt, U., Pupek, M., Ramonet, M., Randa, B., Reichelt, M., Rhee, T. S., Rohwer, J., Rosenfeld, K., Scharffe, D., Schlager, H., Schumann, U., Slemr, F., Sprung, D., Stock, P., Thaler, R., Valentino, F., van Velthoven, P., Waibel, A., Wandel, A., Waschitschek, K., Wiedensohler, A., Xueref-Remy, I., Zahn, A., Zech, U., and Ziereis, H.: Civil Aircraft for the regular investigation of the atmosphere based on an instrumented container: The new CARIBIC system, Atmos. Chem. Phys., p. 24, 2007.

Bundke, U., Berg, M., Houben, N., Ibrahim, A., Fiebig, M., Tettich, F., Klaus, C., Franke, H., and Petzold, A.: The IAGOS-CORE aerosol package: instrument design, operation and performance for continuous measurement aboard in-service aircraft, Tellus B: Chemical and Physical Meteorology, 67, 28 339, https://doi.org/10.3402/tellusb.v67.28339, https://www.tandfonline.com/doi/full/10.3402/tellusb.v67.28339, 2015.

Dee, D. P., Uppala, S. M., Simmons, A. J., Berrisford, P., Poli, P., Kobayashi, S., Andrae, U., Balmaseda, M. A., Balsamo, G., Bauer, P., Bechtold, P., Beljaars, A. C. M., Berg, L. v. d., Bidlot, J., Bormann, N., Delsol, C., Dragani, R., Fuentes, M., Geer, A. J., Haimberger, L., Healy, S. B., Hersbach, H., Hólm, E. V., Isaksen, L., Kållberg, P., Köhler, M., Matricardi, M., McNally, A. P., Monge-Sanz, B. M., Morcrette, J.-J., Park, B.-K., Peubey, C., Rosnay, P. d., Tavolato, C., Thépaut, J.-N., and Vitart, F.: The ERA-Interim reanalysis: configuration and performance of the data assimilation system, Quarterly Journal of the Royal Meteorological Society, 137, 553–597, https://doi.org/10.1002/qj.828, https://rmets.onlinelibrary.wiley.com/doi/abs/10.1002/qj.828, 2011.

DeMott, P. J., Cziczo, D. J., Prenni, A. J., Murphy, D. M., Kreidenweis, S. M., Thomson, D. S., Borys, R., and Rogers, D. C.: Measurements of the concentration and composition of nuclei for cirrus formation, Proceedings of the National Academy of Sciences, 100, 14 655–14 660, https://doi.org/10.1073/pnas.2532677100, http://www.pnas.org/cgi/doi/10.1073/pnas.2532677100, 2003.

Dessler, A. E. and Sherwood, S. C.: ATMOSPHERIC SCIENCE: A Matter of Humidity, Science, 323, 1020–1021, https://doi.org/10.1126/science.1171264, http://www.sciencemag.org/cgi/doi/10.1126/science.1171264, 2009.

Diao, M., Zondlo, M. A., Heymsfield, A. J., Avallone, L. M., Paige, M. E., Beaton, S. P., Campos, T., and Rogers, D. C.: Cloud-scale ice-supersaturated regions spatially correlate with high water vapor heterogeneities, Atmospheric Chemistry and Physics, 14, 2639–2656, https://doi.org/10.5194/acp-14-2639-2014, https://www.atmos-chem-phys.net/14/2639/2014/, 2014.

Filges, A., Gerbig, C., Chen, H., Franke, H., Klaus, C., and Jordan, A.: The IAGOS-core greenhouse gas package: a measurement system for continuous airborne observations of CO_2, CH_4, H_2O and CO, Tellus B: Chemical and Physical Meteorology, 67, 27 989, https://doi.org/10.3402/tellusb.v67.27989, https://www.tandfonline.com/doi/full/10.3402/tellusb.v67.27989, 2015.

https://doi.org/10.5194/acp-2019-573
Preprint. Discussion started: 19 July 2019

Atmospheric Chemistry and Physics Discussions

Fusina, F., Spichtinger, P., and Lohmann, U.: Impact of ice supersaturated regions and thin cirrus on radiation in the midlatitudes, Journal of Geophysical Research: Atmospheres, 112, https://doi.org/10.1029/2007JD008449, https://agupubs.onlinelibrary.wiley.com/doi/abs/10.1029/2007JD008449, 2007.

Gettelman, A., Fetzer, E. J., Eldering, A., and Irion, F. W.: The Global Distribution of Supersaturation in the Upper Troposphere from the Atmospheric Infrared Sounder, Journal of Climate, 19, 6089–6103, https://doi.org/10.1175/JCLI3955.1, http://journals.ametsoc.org/doi/abs/10.1175/JCLI3955.1, 2006.

Gierens, K. and Spichtinger, P.: On the size distribution of ice-supersaturated regions in the upper troposphere and lowermost stratosphere, Annales Geophysicae, 18, 6, 2000.

Gierens, K., Schumann, U., Helten, M., Smit, H., and Marenco, A.: A distribution law for relative humidity in the upper troposphere and lower stratosphere derived from three years of MOZAIC measurements, Annales Geophysicae, 17, 9, 1999.

Held, I. M. and Soden, B. J.: Water Vapor Feedback and Global Warming, Annual Review of Energy and the Environment, 25, 441–475, https://doi.org/10.1146/annurev.energy.25.1.441, https://doi.org/10.1146/annurev.energy.25.1.441, 2000.

Heymsfield, A. J. and Sabin, M., R.: Cirrus Crystal Nucleation by Homogeneous Freezing of Solution Droplets, Journal of the Atmospheric Sciences, 46, 2252–2264, https://doi.org/10.1175/1520-0469(1989)046, 1989.

Holton, J.: An Introduction to Dynamic Meteorology, 5 edn., https://www.elsevier.com/books/an-introduction-to-dynamic-meteorology/holton/978-0-12-384866-6, 2005.

Joos, H., Spichtinger, P., Reutter, P., and Fusina, F.: Influence of heterogeneous freezing on the microphysical and radiative properties of orographic cirrus clouds, Atmospheric Chemistry and Physics, 14, 6835–6852, https://doi.org/10.5194/acp-14-6835-2014, https://www.atmos-chem-phys.net/14/6835/2014/, 2014.

Koop, T., Luo, B., Tsias, A., and Peter, T.: Water activity as the determinant for homogeneous ice nucleation in aqueous solutions, Nature, 406, 611–614, https://doi.org/10.1038/35020537, http://www.nature.com/articles/35020537, 2000.

Krämer, M., Rolf, C., Luebke, A., Afchine, A., Spelten, N., Costa, A., Meyer, J., Zöger, M., Smith, J., Herman, R. L., Buchholz, B., Ebert, V., Baumgardner, D., Borrmann, S., Klingebiel, M., and Avallone, L.: A microphysics guide to cirrus clouds – Part 1: Cirrus types, Atmospheric Chemistry and Physics, 16, 3463–3483, https://doi.org/10.5194/acp-16-3463-2016, https://www.atmos-chem-phys.net/16/3463/2016/, 2016.

Kunz, A., Spelten, N., Konopka, P., Müller, R., Forbes, R. M., and Wernli, H.: Comparison of Fast In situ Stratospheric Hygrometer (FISH) measurements of water vapor in the upper troposphere and lower stratosphere (UTLS) with ECMWF (re)analysis data, Atmospheric Chemistry and Physics, 14, 10 803–10 822, https://doi.org/10.5194/acp-14-10803-2014, https://www.atmos-chem-phys.net/14/10803/2014/, 2014.

Madonna, E., Wernli, H., Joos, H., and Martius, O.: Warm Conveyor Belts in the ERA-Interim Dataset (1979–2010). Part I: Climatology and Potential Vorticity Evolution, Journal of Climate, 27, 3–26, https://doi.org/10.1175/JCLI-D-12-00720.1, http://journals.ametsoc.org/doi/abs/10.1175/JCLI-D-12-00720.1, 2014.

Marenco, A., Thouret, V., Nédélec, P., Smit, H., Helten, M., Kley, D., Karcher, F., Simon, P., Law, K., Pyle, J., Poschmann, G., Wrede, R. V., Hume, C., and Cook, T.: Measurement of ozone and water vapor by Airbus in-service aircraft: The MOZAIC airborne program, an overview, Journal of Geophysical Research: Atmospheres, 103, 25 631–25 642, https://doi.org/10.1029/98JD00977, https://agupubs.onlinelibrary.wiley.com/doi/abs/10.1029/98JD00977, 1998.

Mohler, O., Field, P. R., Connolly, P., Benz, S., Saathoff, H., Schnaiter, M., Wagner, R., Cotton, R., Kramer, M., Mangold, A., and Heymseld, A. J.: Efciency of the deposition mode ice nucleation on mineral dust particles, Atmos. Chem. Phys., p. 15, 2006.

https://doi.org/10.5194/acp-2019-573
Preprint. Discussion started: 19 July 2019

Atmospheric Chemistry and Physics Discussions

Murphy, D. M. and Koop, T.: Review of the vapour pressures of ice and supercooled water for atmospheric applications, Quarterly Journal of the Royal Meteorological Society, 131, 1539–1565, https://doi.org/10.1256/qj.04.94, https://rmets.onlinelibrary.wiley.com/doi/abs/10.1256/qj.04.94, 2005.

Myhre, G., Samset, B. H., Schulz, M., Balkanski, Y., Bauer, S., Berntsen, T. K., Bian, H., Bellouin, N., Chin, M., Diehl, T., Easter, R. C., Feichter, J., Ghan, S. J., Hauglustaine, D., Iversen, T., Kinne, S., Kirkevåg, A., Lamarque, J.-F., Lin, G., Liu, X., Lund, M. T., Luo, G., Ma, X., van Noije, T., Penner, J. E., Rasch, P. J., Ruiz, A., Seland, , Skeie, R. B., Stier, P., Takemura, T., Tsigaridis, K., Wang, P., Wang, Z., Xu, L., Yu, H., Yu, F., Yoon, J.-H., Zhang, K., Zhang, H., and Zhou, C.: Radiative forcing of the direct aerosol effect from AeroCom Phase II simulations, Atmospheric Chemistry and Physics, 13, 1853–1877, https://doi.org/10.5194/acp-13-1853-2013, https://www.atmos-chem-phys.net/13/1853/2013/, 2013.

Müller, S., Hoor, P., Berkes, F., Bozem, H., Klingebiel, M., Reutter, P., Smit, H. G. J., Wendisch, M., Spichtinger, P., and Borrmann, S.: In situ detection of stratosphere-troposphere exchange of cirrus particles in the midlatitudes, Geophysical Research Letters, 42, 949–955, https://doi.org/10.1002/2014GL062556, https://agupubs.onlinelibrary.wiley.com/doi/abs/10.1002/2014GL062556, 2015.

Neis, P. R.: Water vapour in the UTLS - Climatologies and Transport, Ph.D. thesis, Johannes Gutenberg University, Mainz, 2017.

Petzold, A., Thouret, V., Gerbig, C., Zahn, A., Brenninkmeijer, C. A. M., Gallagher, M., Hermann, M., Pontaud, M., Ziereis, H., Boulanger, D., Marshall, J., Nédélec, P., Smit, H. G. J., Friess, U., Flaud, J.-M., Wahner, A., Cammas, J.-P., Volz-Thomas, A., and IAGOS TEAM: Global-scale atmosphere monitoring by in-service aircraft – current achievements and future prospects of the European Research Infrastructure IAGOS, Tellus B: Chemical and Physical Meteorology, 67, 28 452, https://doi.org/10.3402/tellusb.v67.28452, https://www.tandfonline.com/doi/full/10.3402/tellusb.v67.28452, 2015.

Reutter, P., Škerlak, B., Sprenger, M., and Wernli, H.: Stratosphere–troposphere exchange (STE) in the vicinity of North Atlantic cyclones, Atmospheric Chemistry and Physics, 15, 10 939–10 953, https://doi.org/10.5194/acp-15-10939-2015, https://www.atmos-chem-phys.net/15/10939/2015/, 2015.

Riese, M., Ploeger, F., Rap, A., Vogel, B., Konopka, P., Dameris, M., and Forster, P.: Impact of uncertainties in atmospheric mixing on simulated UTLS composition and related radiative effects, Journal of Geophysical Research: Atmospheres, 117, https://doi.org/10.1029/2012JD017751, https://agupubs.onlinelibrary.wiley.com/doi/abs/10.1029/2012JD017751, 2012.

Rohs, S., Schiller, C., Riese, M., Engel, A., Schmidt, U., Wetter, T., Levin, I., Nakazawa, T., and Aoki, S.: Long-term changes of methane and hydrogen in the stratosphere in the period 1978–2003 and their impact on the abundance of stratospheric water vapor, Journal of Geophysical Research: Atmospheres, 111, https://doi.org/10.1029/2005JD006877, https://agupubs.onlinelibrary.wiley.com/doi/abs/10.1029/2005JD006877, 2006.

Solomon, S., Rosenlof, K. H., Portmann, R. W., Daniel, J. S., Davis, S. M., Sanford, T. J., and Plattner, G.-K.: Contributions of Stratospheric Water Vapor to Decadal Changes in the Rate of Global Warming, Science, 327, 1219–1223, https://doi.org/10.1126/science.1182488, http://www.sciencemag.org/cgi/doi/10.1126/science.1182488, 2010.

Spichtinger, P.: Shallow cirrus convection – a source for ice supersaturation, Tellus A: Dynamic Meteorology and Oceanography, 66, 19 937, https://doi.org/10.3402/tellusa.v66.19937, https://www.tandfonline.com/doi/full/10.3402/tellusa.v66.19937, 2014.

Spichtinger, P. and Leschner, M.: Horizontal scales of ice-supersaturated regions, Tellus B: Chemical and Physical Meteorology, 68, 29 020, https://doi.org/10.3402/tellusb.v68.29020, https://www.tandfonline.com/doi/full/10.3402/tellusb.v68.29020, 2016.

Spichtinger, P., Gierens, K., and Read, W.: The global distribution of ice-supersaturated regions as seen by the Microwave Limb Sounder, Quarterly Journal of the Royal Meteorological Society, 129, 3391–3410, https://doi.org/10.1256/qj.02.141, https://rmets.onlinelibrary.wiley.com/doi/abs/10.1256/qj.02.141, 2003.

https://doi.org/10.5194/acp-2019-573
Preprint. Discussion started: 19 July 2019

Atmospheric Chemistry and Physics Discussions

Thompson, A. M.: The Oxidizing Capacity of the Earth's Atmosphere: Probable Past and Future Changes, Science, 256, 1157–1165, https://doi.org/10.1126/science.256.5060.1157, http://www.sciencemag.org/cgi/doi/10.1126/science.256.5060.1157, 1992.

Thouret, V., Cammas, J.-P., Sauvage, B., Athier, G., Zbinden, R., Nedelec, P., Simon, P., and Karcher, F.: Tropopause referenced ozone climatology and inter-annual variability (1994–2003) from the MOZAIC programme, Atmos. Chem. Phys., 6, 19, 2006.

Tompkins, A. M., Gierens, K., and Rädel, G.: Ice supersaturation in the ECMWF integrated forecast system, Quarterly Journal of the Royal Meteorological Society, 133, 53–63, https://doi.org/10.1002/qj.14, https://rmets.onlinelibrary.wiley.com/doi/abs/10.1002/qj.14, 2007.

Uma, K. N., Das, S. K., and Das, S. S.: A climatological perspective of water vapor at the UTLS region over different global monsoon regions: observations inferred from the Aura-MLS and reanalysis data, Climate Dynamics, 43, 407–420, https://doi.org/10.1007/s00382-014-2085-9, http://link.springer.com/10.1007/s00382-014-2085-9, 2014.

Zhan, R. and Wang, Y.: Contribution of tropical cyclones to stratosphere-troposphere exchange over the northwest Pacific: Estimation based on AIRS satellite retrievals and ERA-Interim data: CONTRIBUTION BY TCS TO STE OVER WNP, Journal of Geophysical Research: Atmospheres, 117, n/a–n/a, https://doi.org/10.1029/2012JD017494, http://doi.wiley.com/10.1029/2012JD017494, 2012.